

LiDAR-Generated Images Derived Keypoints Assisted Point Cloud Registration Scheme in Odometry Estimation

Haizhou Zhang^{*†‡}, Xianjia Yu^{*‡}, Sier Ha[‡], Tomi Westerlund[‡]

^{*}These authors contributed equally to this work.

[†]School of Information Science and Technology, Fudan University, China

[‡]Turku Intelligent Embedded and Robotic Systems (TIERS) Lab, University of Turku, Finland.

Emails: ¹{haizhouzhang21}@m.fudan.edu.cn, ²{xianjia.yu, sierha, toveve}@utu.fi

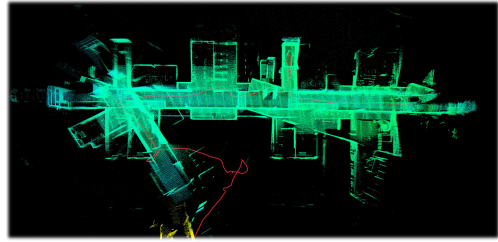
arXiv:2309.10436v1 [cs.RO] 19 Sep 2023

Abstract—Keypoint detection and description play a pivotal role in various robotics and autonomous applications including visual odometry (VO), visual navigation, and Simultaneous localization and mapping (SLAM). While a myriad of keypoint detectors and descriptors have been extensively studied in conventional camera images, the effectiveness of these techniques in the context of LiDAR-generated images, i.e. reflectivity and ranges images, has not been assessed. These images have gained attention due to their resilience in adverse conditions such as rain or fog. Additionally, they contain significant textural information that supplements the geometric information provided by LiDAR point clouds in the point cloud registration phase, especially when reliant solely on LiDAR sensors. This addresses the challenge of drift encountered in LiDAR Odometry (LO) within geometrically identical scenarios or where not all the raw point cloud is informative and may even be misleading. This paper aims to analyze the applicability of conventional image keypoint extractors and descriptors on LiDAR-generated images via a comprehensive quantitative investigation. Moreover, we propose a novel approach to enhance the robustness and reliability of LO. After extracting key points, we proceed to downsample the point cloud, subsequently integrating it into the point cloud registration phase for the purpose of odometry estimation. Our experiment demonstrates that the proposed approach has comparable accuracy but reduced computational overhead, higher odometry publishing rate, and even superior performance in scenarios prone to drift by using the raw point cloud. This, in turn, lays a foundation for subsequent investigations into the integration of LiDAR-generated images with LO. Our code is available in the github: <https://github.com/TIERS/ws-lidar-as-camera-odom>.

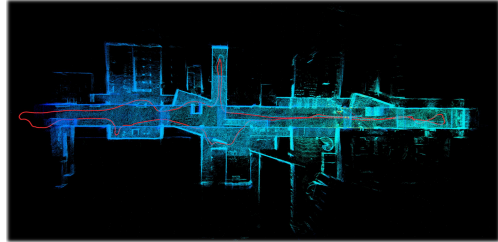
Index Terms—LiDAR; LiDAR-generated images; keypoint detector and descriptor; Point cloud registration; LiDAR Odometry; LO; Lidar-as-a-camera;

I. INTRODUCTION

LiDAR technology has become a primary sensor for facilitating advanced situational awareness in the domains of robotics and autonomous systems ranging from LiDAR Odometry (LO), Simultaneous Localization and Mapping (SLAM), object detection and tracking, as well as navigation. Among these applications, LO, as a fundamental component in robotics has significantly drawn our attention. Extensive research efforts have focused on the integration of diverse sensors, including Inertial Measurement Units (IMUs), to



(a) Raw point cloud with point cloud matching approach (KISS-ICP)



(b) Our proposed LiDAR-generated keypoint extraction-based approach

Fig. 1: Samples of LiDAR odometry results run in our experiment

bolster LO performance. However, in scenarios where LiDAR data lacks geometric distinctness or even contains misleading information, the process of point cloud registration continues to present challenges in achieving precise estimations and even causing drift in certain cases (Fig 1a).

Notably, recent years have witnessed substantial progress in LiDAR technology, marked by the emergence of numerous high-resolution spinning and solid-state LiDAR devices offering various modalities of sensor data [1], [2]. The increased density of the point cloud brings a challenge for point cloud registration with a significant computation overhead, especially for devices with limited computational resources.

Within the aforementioned modalities, LiDAR-generated images, including reflectivity images, range images, and near-infrared images, have introduced the potential to apply conventional camera image processing techniques to LiDAR-generated images. These images are low-resolution but possi-

bly panoramic and exhibit heightened resilience and robustness in challenging environments, such as those characterized by fog and rain, compared to conventional camera images. Additionally, these images can potentially provide crucial information for point cloud registration when there is a deficiency of geometric data or the raw point cloud lacks useful information so as to avoid drift (Fig. 1b).

Keypoint detectors and descriptors have found extensive utility across diverse domains within visual tasks such as place recognition, scene reconstruction, Visual Odometry (VO), Visual Simultaneous Localization and Mapping (VSLAM), and Visual Inertial Odometry (VIO). Nevertheless, there remains a lack of investigation into the performance of extant keypoint detectors and descriptors when applied to LiDAR-generated imagery.

Contemporary methodologies for Visual Odometry (VO) or Visual Inertial Odometry (VIO) rely significantly on the operability of visual sensors, necessitating knowledge of camera intrinsics to facilitate Structure from Motion (SfM) – a requisite not met by LiDAR-generated images. This poses the difficulty of extracting key points from LiDAR-generated images in a certain way to further apply in the odometry estimation.

Therefore, to address the above issues, in this study,

- i) We investigate the efficacy of the existing keypoint detectors and descriptors on LiDAR-generated images with multiple specialized metrics providing a quantitative evaluation.
- ii) We conduct an extensive study of the optimal resolution and interpolation approaches for enhancing the low-resolution LiDAR-generated data to extract key points more effectively.
- iii) we propose a novel approach by leverages the detected key points and their neighbors to extract a reliable point cloud (downsampling) for the purpose of point cloud registration with reduced computational overhead and fewer deficiencies in valuable point acquisition.

The structure of this paper is as follows. In Section II, we survey the recent progress on keypoint detectors and descriptors including approaches and metrics, point cloud matching, and the status of LO. Section III provides an overview of the quantitative evaluation of the existing keypoint detectors and descriptors, the proposed keypoint-assisted point cloud registration, and others. Section IV demonstrates the experimental results in detail. In the end, we conclude the work and sketch out some future research directions in Section V.

II. RELATED WORK

In this section, we commence by presenting a comprehensive review of the prevailing detector and descriptor algorithms documented in the literature. Subsequently, a brief summary of the current advancements in the domain of LiDAR-imaged techniques is offered. We conclude with a concise analysis of the leading algorithms for point cloud registration in LO.

A. Keypoint Detector and Descriptor

In recent years, there have been multiple widely applied detectors and descriptors in the field of computer vision. As illustrated in Table I, we've captured the essential characteristics of different detectors and descriptors.

Harris detector [3] can be seen as an enhanced version of Moravec's corner detector [4] [5]. It's used to identify corners in an image, which are the regions with large intensity variations in multiple directions. The Shi-Tomasi Corner Detector[6], is an improvement upon the Harris Detector with a slight modification in the corner response function that makes it more robust and reliable in certain scenarios. The Features from Accelerated Segment Test (FAST)[7] algorithm operates by examining a circle of pixels surrounding a candidate pixel and testing for a contiguous segment of pixels that are either significantly brighter or darker than the central pixel.

For descriptor-only algorithms, Binary Robust Independent Elementary Features (BRISK) [8] utilizes a set of binary tests on pairs of pixels within a patch surrounding one key point. Fast Retina Keypoint (FREAK) [9] is inspired by the human visual system, which constructs a retinal sampling pattern that is more densely sampled towards the center and sparser towards the periphery. Then it compares pairs of pixels within this pattern to generate a robust binary descriptor.

With respect to the combined detector-descriptor algorithms, the Scale-Invariant Feature Transform (SIFT) [10] [11] detects key points by identifying local extrema in the Difference of Gaussian scale-space pyramid, then computes a gradient-based descriptor for each keypoint. Speeded-Up Robust Features (SURF) [12] is designed to address the computational complexity of SIFT while maintaining robustness to various transformations. Binary Robust Invariant Scalable Keypoints (BRISK) [13] uses a scale-space FAST [7] detector to identify key points and computes binary descriptors based on a sampling pattern of concentric circles. Oriented FAST and Rotated BRIEF (ORB) [14] extends the FAST detector with a multi-scale pyramid and computes a rotation-invariant version of the BRIEF [8] descriptor, aiming to provide a fast and robust alternative to SIFT and SURF. Accelerated-KAZE (AKAZE) [15] employs a Fast Explicit Diffusion scheme to accelerate the detection process and computes a Modified Local Difference Binary (M-LDB) descriptor [16] for robust matching.

The emergence of deep learning (DL) techniques, particularly convolutional neural networks (CNN) [17][18], has revolutionized computer vision, over the last decade. SuperPoint[19] detector employs a fully CNN to predict a set of keypoint heatmaps, where each heatmap corresponds to an interest point's probability at a given pixel location. Then, the descriptor part generates a dense descriptor map for the input image by predicting a descriptor vector at each pixel location.

To sum up, while numerous detector and descriptor algorithms have gained popularity, it is imperative to note that they have primarily been designed for traditional camera images, not LiDAR-based images. Consequently, it's of paramount

importance for this study to identify the algorithms that maintain efficacy for LiDAR-based images.

TABLE I: Keypoint detectors and descriptors

Method	Detector	Descriptor	Description
Harris	✓		Corner detection method focusing on local image variations.
Shi-Tomasi	✓		Variation of Harris with modification in the response function to be more robust.
FAST	✓		Efficient corner detection for real-time applications.
FREAK		✓	Robust to transformations, based on human retina's structure.
BRIEF		✓	Efficient short binary descriptor for key points.
SIFT	✓	✓	Invariant to scale, orientation, and partial illumination changes.
SURF	✓	✓	Addresses the computational complexity of SIFT while maintaining robustness.
BRISK	✓	✓	Faster binary descriptor method, efficient compared to SIFT/SURF.
ORB	✓	✓	Combines FAST detection and BRIEF descriptor, commonly used now.
AKAZE	✓	✓	Builds on KAZE but faster, good for wide baseline stereo correspondence.
Superpoint	✓	✓	A state-of-the-art AI approach that exhibits superior performance when applied to traditional camera images.

B. LiDAR-Generated Images in Robotics

Within the realm of robotics, some studies over the years have delved into the utilization of LiDAR-based images. But before exploring specific applications, it is vital to know the process by which range images, signal images are generated from point cloud, as detailed in [20], [21]. And it's also essential to understand the effectiveness of LiDAR-based images, through an extensive evaluation in the article [22], showing that LiDAR-based images have remarkable resilience to seasonal and environmental variations.

Perception emerges as the indisputable first step in the use of LiDAR within robotics. In [23], Ouster introduced their work, to explain the possibility of using LiDAR as a camera. They demonstrate the effectiveness of car and road segmentation by putting the LiDAR-based image into a pretrained DL model. In the work [24], Tsiourva et al. proposed a saliency detection model based on LiDAR-generated images. In the model, the attributes of reflectivity, intensity, range, and ambient images are carefully contrasted and analyzed. After several advanced image processing steps, multiple conspicuity maps are created. These maps help make a unified saliency map, which identifies and emphasizes the most distinct objects in the image. In the research [25], Sier et al. explored using LiDAR-as-a-camera sensors to track Unmanned Aerial Vehicles (UAVs) in GNSS-

denied environments, fusing LiDAR-generated images and point clouds for real-time accuracy. The work [26] explores the potential of general-purpose deep learning perception algorithms, specifically detection and segmentation neural networks, based on LiDAR-generated images. The study provides both a qualitative and quantitative analysis of the performance of a variety of neural network architectures, proving that the DL models built for visual camera images also offer significant advantages when applied to LiDAR-generated images.

Delving deeper into subsequent applications, for example, localization, research in [27], explores the problem of localizing mobile robots and autonomous vehicles within a large-scale outdoor environment map, by leveraging range images produced by 3D LiDAR.

C. Evaluation Metrics for Keypoint Detectors and Descriptors

The efficacy of detector and descriptor algorithms is typically assessed through some specific evaluation metrics. As illustrated in Table II, the first three metrics, Number of Keypoints, Computational Efficiency, and Robustness of Detector are straightforward to comprehend and implement, and also widely adopted in numerous studies [28] [12] [29]. For instance, the Robustness of the Detector [30] is implemented by contrasting key points before and after the transformations like *scaling*, *rotation*, and *Gaussian noise interference*.

When assessing the precision of the entire algorithmic procedure, which is prioritized by the majority of tasks, the prevalent metrics often necessitate benchmark datasets, such as KITTI [31], HPatches [32]. These datasets either provide the transformation matrix between images or directly contain the key point ground truth. For example, in Mukherjee et al.'s study [33], one crucial metric: "Precision", is defined as *correct matches/all detected matches*, where correct matches are ascertained through the geometric verification based on a known camera position provided by dataset [34]. Similarly, in this recent work [35], the evaluation tasks including "keypoint verification", "image matching", and "keypoint retrieval", all rely on the homography matrix between images in the benchmark dataset [32].

Nevertheless, given that research predicated on LiDAR images is at a nascent stage, there exists no benchmark dataset in the field of LiDAR-based images. And the effort required for data labeling [36] [37] to produce such a dataset is considerable and challenging. To bridge this gap, we select multiple key evaluation metrics: Match ratio, Match score, and Distinctiveness, as shown in Table II from previous studies. Match Ratio [33] is quantitatively defined as *number of matches/number of key points*. A high Match Ratio can suggest that the algorithm is adept at identifying and correlating distinct features; While the exact homography matrix between images remains unknown when lacking benchmark datasets, it can be approximated using mathematical methodologies from two point sets. This computed homography can subsequently be utilized to find correct matches. And *number of estimated correct matches/number of matches* is denoted as Match Score in our work; And Distinctiveness is computed as follows:

TABLE II: Metrics for evaluating keypoint detectors and descriptors

Metrics	Description
Number of Keypoints	A high number of key points can always lead to more detailed image analysis and better performance in subsequent tasks like object recognition.
Computational Efficiency	Computational efficiency remains paramount in any computer vision algorithms. We gauge this efficiency by timing the complete detection, description, and matching process.
Robustness of Detector	An efficacious detector should recognize identical key points under varying conditions such as scale, rotation, and Gaussian noise interference.
Match Ratio	The ratio of successfully matched points to the total number of detected points, offers insights into the algorithm’s capability in identifying and relating unique keypoints.
Match Score	A homography matrix is estimated from two point sets, to distinguish spurious matches, then the algorithm precision is quantified by the inlier ratio.
Distinctiveness	Distinctiveness entails that the key points isolated by a detection algorithm should exhibit sufficient uniqueness for differentiation among various key points.

For every image, the k-nearest neighbors algorithm, with $k=2$, is employed to identify the two best matches [10]. If the descriptor distance of the primary match is notably lower than that of the secondary match, it demonstrates the algorithm’s competence in recognizing and describing highly distinctive key points. Consequently, this defines the metric: Distinctiveness.

D. 3D Point Cloud Downsampling

Point cloud downsampling is crucial in operating LO or SLAM within a computation-constrained device. Nowadays, there is a substantial of work focusing on the employment of DL networks, for example, a lightweight transformer [38]. Other approaches utilized various filters in order to achieve not only point cloud downsampling but also denoising [39].

E. 3D Point Cloud Matching in LO

LO has been widely studied yet challenging due to the complexity of the environment in the robotic field. Contemporary research endeavors have witnessed a notable surge in efforts integrating supplementary sensors, such as Inertial Measurement Units (IMUs), aimed at augmenting the precision and resilience of LO. However, as we focus on the point cloud registration phase of LO, this is out of the scope of the related work of this part. We primarily discuss the solely LiDAR-based LO. Among these solely LiDAR-based approaches, LOAM [40] as a popular matching-based SLAM and LO approach has encouraged a great amount of other LO approaches including Lego-LOAM [41] and F-LOAM [42].

Point cloud matching or registration constitutes the key component in LO. Since its inception approximately three decades ago, the Iterative Closest Point (ICP) algorithm, as introduced by Besl and McKay [43], has spawned numerous variants. These include notable adaptations such as Voxelized Generalized ICP (GICP)[44], CT-ICP[45], and KISS-ICP [46]. Among these ICP iterations, KISS-ICP, denoting “keep it small and simple”, distinguishes itself by providing a point-to-point ICP approach characterized by robustness and accuracy in pose estimation. Furthermore, the Normal Distributions Transform (NDT) [47] represents another prominent point cloud registration technique frequently employed in LO research. As the latest ICP approach, KISS-ICP is the designated methodology for the point cloud registration we adopted in this study.

III. METHODOLOGY

In this section, we first introduce the dataset we used. Then, we describe our experimental procedure in detail.

A. Dataset

For the evaluation of keypoint detectors and descriptors and our proposed approach, we utilized the published open-source dataset for multi-modal LiDAR sensing [1]. The dataset consists of various LiDARs and among them, Ouster LiDAR provides not only point cloud but also its generated images. The Ouster LiDAR applied in the dataset is OS0-128 with its detailed specifications shown in Table III.

TABLE III: Specifications of Ouster OS0-128.

	IMU	Type	Channels	Image Resolution	FoV	Angular Resolution	Range	Freq	Points
Ouster OS0-128	ICM-20948	spinning	128	2048 × 128	360° × 90°	V : 0.7°, H : 0.18°	50m	10Hz	2,621,440 pts/s

The images generated by OS0-128 shown in Fig. 2 include signal images, reflectivity images, near-infrared images, and range images with its expansive $360^\circ \times 90^\circ$ field of view. Signal images are representations of the signal strength of the light returned to the sensor for a given point, which depends on various factors, such as the angle of incidence, the distance from the sensor, and the material properties of the object. In near-infrared images, each pixel’s intensity is represented by the amount of detected photons that are not emitted by the sensor’s own laser pulse but may come from sources such as sunlight or moonlight. And every pixel in a reflectivity image represents the calculated calibrated reflectivity. Then, range

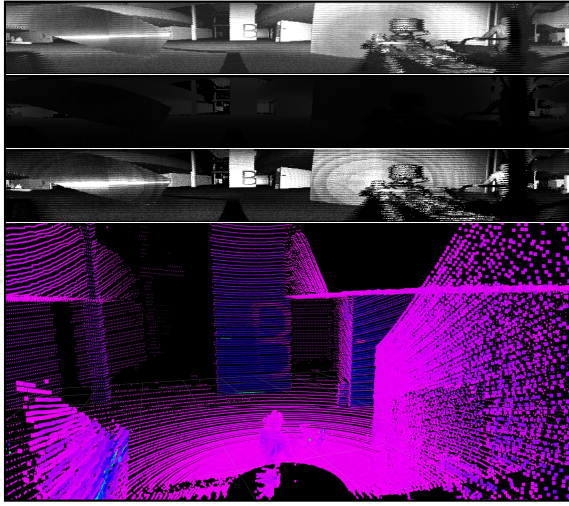


Fig. 2: Samples of LiDAR-Generated Images, from above to bottom are signal image, range image, reflectivity image, and point cloud.

images demonstrate the distance from the sensor to objects in the environment.

As indicated by the findings of our previous research, signal images have exhibited superior performance in the execution of conventional DL tasks within the domain of computer vision [26]. In light of this, for the first two parts of our experiment, we opt to employ signal images from the "indoor_01_square" scene provided by the dataset, which is a scene that spans 114 seconds and comprises 1146 image messages.

B. Optimal Preprocessing Configuration Searching for LiDAR-Generated Images

LiDAR-generated images at hand are typically panoramic but low-resolution. Moreover, these images often exhibit a substantial degree of noise. This prompts a concern of utilizing the original images for facilitating the functionality evaluation of the keypoint detector and descriptor algorithms. And our preliminary experiments have evinced unsatisfactory performance across an array of detectors and descriptors when employing the unaltered original LiDAR-generated images. To identify the optimal resolution and interpolation methodology for augmenting image resolution, an extensive comparative experiment was conducted.

In this part, we implement an array of interpolation techniques on the original images, employing an extensive spectrum of image resolution combinations. The interpolation methodologies encompass bicubic interpolation (CUBIC), Lanczos interpolation over 8x8 neighborhood (LANCZOS4), resampling using pixel area relation (AREA), nearest neighbor interpolation (NEAREST), and bilinear interpolation (LINEAR). The primary procedure of the preprocessing is elucidated in Algorithm 1.

More specifically, we iterate a range of image dimensions and interpolation methods in conjunction with the suite of detector and descriptor algorithms designated for evaluation.

Algorithm 1: Preprocessing configuration evaluation

Input:

N number of signal images: $\{S_i\}, i \sim N$;

Interpolation methods:

$IA = \{CUBIC, LANCZOS4, AREA, NEAREST, LINEAR\}$;

Targeted Width:

$TW = \{min : 512; max : 4096; step : 128\}$;

Targeted Height:

$TH = \{min : 32; max : 256; step : 32\}$;

Detectors and descriptors:

$DET =$

$\{SURF, SIFT, SHITOMASI, HARRIS, BRISK, FAST, AKAZE, ORB\}$;

$DES =$

$\{FREAK, SIFT, BRISK, SURF, BRIEF, AKAZE, ORB\}$;

Output: Metrics

```

foreach interpolation approach in  $IA$  do
  foreach width in  $TW$  do
    foreach height in  $TH$  do
      foreach det in  $DET$  and des in  $DES$  do
        foreach  $S_i$  do
          Calculate the value of
            aforementioned metrics;
          Save the calculated value;
        endforeach
      endforeach
    endforeach
  endforeach
endforeach
Analyze the metric values.

```

Each iteration involves a rigorous evaluation of a comprehensive metrics set detailed in Table II. Following a quantitative analysis, we compute mean values for these metrics. This extensive assessment aims to identify the optimal preprocessing configuration that offers a balanced performance for different keypoint detectors and descriptors.

C. Keypoint Detectors and Descriptors for LiDAR-Generated Images

The evaluation workflow of detector-descriptor algorithms typically comprises three stages including feature extraction, keypoint description, and keypoint matching between successive image frames. In this section, the specific procedures for executing these stages in our experimental setup will be elaborated upon.

1) *Designated Keypoint Detector and Descriptor*: An extensive array of keypoint detectors and descriptors, as detailed in Table I from Section II-A, were investigated. The employed keypoint detectors include SHITOMASI, HARRIS, FAST, BRISK, SIFT, SURF, AKAZE, and ORB. Additionally, we integrated Superpoint, a DL-based keypoint detector, into our methodology. The keypoint descriptors implemented in our experiment are BRISK, SIFT, SURF, BRIEF, FREAK, AKAZE, ORB.

2) *Key Points Matching between Images*: Keypoint matching, the final stage of the detector-descriptor workflow, focuses on correlating key points between two images, which is essential for establishing spatial relationships and forming a coherent scene understanding. The smaller the distance of the descriptors between two points, the more likely it is that they are the same point or object between two images. In our implementation, we employ a technique termed “brute-force match with cross check”, which means for a given descriptor \mathcal{D}_A in image A and another descriptor \mathcal{D}_B in image B , a valid correspondence requires that both descriptors recognize each other as their closest descriptors.

3) *Selected Evaluation Metrics*: As explained in Section II-C, we have opted not to rely on ground truth-based evaluation methodologies due to the lack of benchmark datasets and the substantial labor involved in data labeling. Instead, we combined some specially-designed metrics that are independent of ground truth, together with several intuitive metrics, to form the complete indicators listed in Table II. To our best understanding, this represents the most extensive set of evaluation metrics currently available in the absence of a benchmark dataset.

4) *Evaluation Process*: The flowchart shown in Algorithm 2 below provides an outline of the steps carried out by the program. Two nested loops are employed to iterate over different detector-descriptor pairs. For each image, the algorithm detects and describes its keypoints. If more than one image has been processed, keypoints from the current image are matched to the previous one. And metrics are placed in corresponding positions to assess the algorithm’s performance.

D. LiDAR-Generated Image Keypoints Assisted Point Cloud Registration

1) *Selected Data*: The selected data for the evaluation from the dataset mentioned in Section III-A includes indoor and outdoor environments. The outdoor environment are from the normal road, denoted as “Open road”, and a forest, denoted as “Forest”. The indoor data include a hall in a building, denoted as “Hall (large)”, and two rooms, denoted as “Lab space (hard)”, and “Lab space (easy)”.

2) *Point Cloud Matching Approach*: In this part, we applied KISS-ICP¹ as our point cloud matching approach. It provides also the odometry information, affording us the means to assess the efficacy of our point cloud downsampling approach through an examination of a positioning error, namely translation error and rotation error. To generalize our proposed approach, we tested an NDT-based simple SLAM program² as well.

3) *Proposed Method for Point Cloud Downsampling*: Following the preprocessing of LiDAR-generated images outlined in Section III-C, we derive optimal configurations for the keypoint detectors and descriptors. Utilizing these configurations as a foundation, we establish the workflow of our proposed

Algorithm 2: Overall evaluation pipeline of keypoint detectors and descriptors

Input:

N number of signal images: $\{S_i\}, i \sim N$;

$DET =$

$\{SURF, SIFT, SHITOMASI, HARRIS, BRISK, FAST, AKAZE, ORB\}$;

$DES =$

$\{FREAK, SIFT, BRISK, SURF, BRIEF, AKAZE, ORB\}$;

Output: Metrics

foreach *Detector* in DET **do**

foreach *Descriptor* in DES **do**

foreach S_i **do**

 Preprocess the image S_i by the method in Algorithm 1;

 Detect keypoints;

 Measure the number of keypoints: N_{kp} ;

 Apply different transformations to image S_i , then calculate robustness: R_{rot} ,

R_{scale}, R_{blur} ;

if $i > 1$ **then**

 Match keypoints between successive frames;

 Record the algorithm running time RT as Computational Efficiency;

 Calculate Match Ratio, Match Score, Distinctiveness;

 Analyze the metric values.

methodology, illustrated in Fig. 3. Within this process, we conduct distinct preprocessing procedures for both the range and signal images, employing them individually for keypoint detection and descriptor extraction. Subsequently, we combine the key points obtained from both images and search the K nearest points to each of these key points. We systematically varied K within the range of 3 to 7, adhering to a maximum threshold of 7 to align with our primary objective of downsampling the point cloud. Consequently, we find the corresponding point cloud of the key points and their neighbors within the raw point cloud, thereby constituting the downsampled point cloud.

In our analysis, we examined not only the positional error but also the rotational error, computational resource utilization, downsampling-induced alterations in point cloud density, and the publishing rate of LO.

E. Hardware and Software Information

Our experiments are run on the ROS Noetic on the Ubuntu 20.04 system. The platform is equipped with an i7 8-core 1.6 GHz CPU and an Nvidia GeForce MX150 graphics card. Primarily, we used libraries like OpenCV and PCL. Note, that we have used some non-free copyright-protected algorithms from OpenCV, such as SURF, just for research.

¹<https://github.com/PRBonn/kiss-icp.git>

²https://github.com/Kin-Zhang/simple_ndt_slam.git

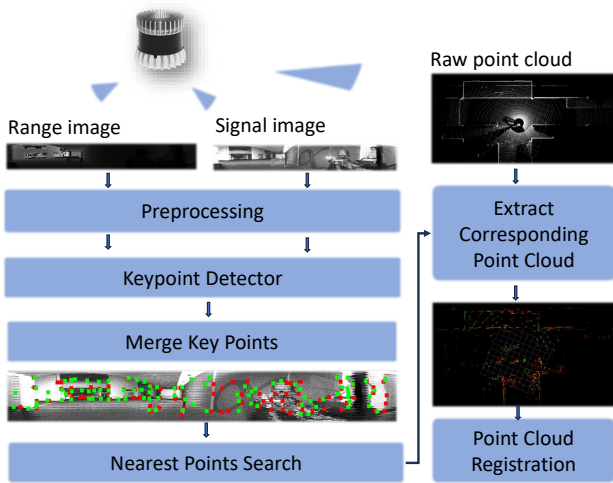


Fig. 3: The process of the proposed LiDAR-generated images assisted point cloud registration

The assessment of keypoint-based point cloud downsampling was conducted on a Lenovo Legion notebook equipped with the following specifications: 16 GB RAM, a 6-core Intel i5-9300H processor (2.40 GHz), and an Nvidia GTX 1660Ti graphics card (boasting 1536 CUDA cores and 6 GB VRAM). Within this study, our primary focus was on the evaluation of the two open-source algorithms delineated in subsection III-D2, namely, KISS-ICP and Simple-NDT-SLAM. It is imperative to highlight that a consistent voxel size of 0.2 m was employed for both algorithms. Our project is primarily written in C++ (including the DL approach, Superpoint), publicly available in GitHub ³.

IV. EXPERIMENT RESULT

Through this section, we first cover the final results of our exploration of the preprocessing workflow of LiDAR-based images. Subsequently, an in-depth analysis of keypoint detectors and descriptors for LiDAR-based images is conducted. Then, a detailed quantitative assessment of the performance of LO facilitated by LiDAR-generated image keypoints is presented.

A. Results of preprocessing methods for LiDAR-generated image

TABLE IV: Evaluation metrics under different interpolation approaches.

Interpolation	Robustness of (rotation, scaling, noise)	Distinctiveness	Matching Score
AREA	(0.81,0.106,0.574)	0.309	0.415
CUBIC	(0.82 ,0.121,0.569)	0.292	0.408
LANCZOS4	(0.819, 0.127 ,0.559)	0.286	0.405
NEAREST	(0.818,0.128,0.573)	0.275	0.401
LINEAR	(0.815,0.1, 0.583)	0.314	0.415

As elucidated in Section II-C, Distinctiveness and Match Score are considered as paramount measures for the overall accuracy of the entire algorithm pipeline. Consequently, in

³<https://github.com/TIERS/ws-lidar-as-camera-odom>

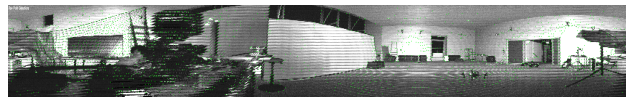
scenarios where different sizes and interpolation methods show peak performance on different metrics, these two metrics are our primary concern. Based on such an criteria, the size **1024 x 64** demonstrated better performance across all detectors and descriptors methods. Then in Table IV, our evaluation also revealed that the **linear** interpolation method yielded the most optimal results among the various interpolation techniques.

TABLE V: Evaluation metrics under different resized resolutions.

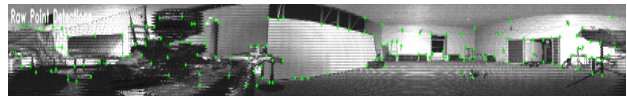
Size	Robustness of (rotation, scaling, noise)	Distinctiveness	Matching Score
512x32	(0.856 , 0.157 ,0.551)	0.267	0.366
896x128	(0.827,0.156,0.591)	0.37	0.515
896x256	(0.843,0.146, 0.663)	0.309	0.486
1024x64	(0.809,0.124,0.54)	0.427	0.53
1024x128	(0.832,0.147,0.584)	0.372	0.504
1024x256	(0.851,0.134,0.659)	0.32	0.483
1280x64	(0.798,0.116,0.527)	0.41	0.5
1280x128	(0.823,0.138,0.575)	0.353	0.479
1280x256	(0.849,0.127,0.652)	0.301	0.464
1920x128	(0.808,0.124,0.553)	0.321	0.436
1920x256	(0.844,0.114,0.644)	0.274	0.43
2048x128	(0.799,0.129,0.544)	0.309	0.425
2048x256	(0.837,0.119,0.633)	0.263	0.421
2560x128	(0.802,0.111,0.547)	0.294	0.4
2560x256	(0.842,0.106,0.644)	0.249	0.401
4096x128	(0.799,0.087,0.557)	0.257	0.339

The findings in Table V, also suggest that there is a clear advantage in properly reducing the size of an image as opposed to enlarging it. Additionally, in the process of image downscaling, one pixel often corresponds to several pixels in original image. So overly downsampled images might lead to substantial deviations in the detected key points when re-projected to their original positions, suggesting that extreme image size reductions should be avoided.

And here is a more intuitive result to show that how reducing the size of a image is far better than enlarging it. In Fig. 4a and Fig. 4b, Superpoint detectors identify keypoints as green dots. The enlarged image Fig. 4a displays many disorganized points. Conversely, the downsampled image Fig. 4a, reveals distinct keypoints, such as room corners and the points where various planes of objects meet. Note that we resized the two images for paper readability, originally, their sizes varied.



(a) Detect key points in an enlarged image.



(b) Detect key points in a downsampled image.

Fig. 4: Keypoint detected in the resized signal images

B. Results of Keypoint Detectors and Descriptors For LiDAR Image

In Fig. 5, which is a metric that only related to detectors, FAST and BRISK algorithms detected the highest number of keypoints, but there were significant fluctuations in the counts.

Comparatively, AKAZE, ORB, and Superpoint identified a reduced number of keypoints, but the consistency was notable.

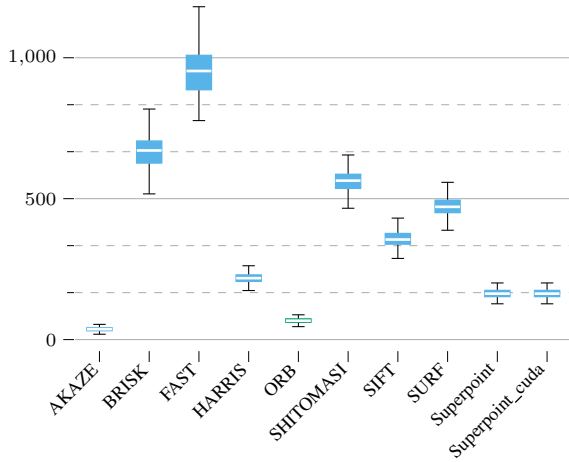


Fig. 5: Number of key points

Fig. 6 depicts the Computational Efficiency, where the majority of the algorithms operate in less than 50 ms. After CUDA enabled, SuperPoint runs significantly faster with minimal variance. Among all algorithms, BRISK is the most time-consuming, just using BRISK solely as a descriptor with other detectors will hinder the overall efficiency.

Fig. 7 shows the Robustness of Detector. Superpoint consistently demonstrates robust performance across various transformations. Among conventional detectors, AKAZE has proven effective, especially in handling rotated transformations and noise interference. And most detectors, exhibit marked poor performance under scale invariance. The horizontal textures inherent in LiDAR-based images might explain such weakness: when the images are enlarged, these textures can be erroneously detected as keypoints.

As emphasized in Section II-C, a multitude of keypoint detections and rapid matches could be useless if their accuracy is not guaranteed. Therefore, Match Ratio, Match Score, and Dinctiveness, which pertain to algorithmic accuracy, can be regarded as the most pivotal indicators across various application perspectives. Fig. ??, Fig. ??, and Fig. ?? present the results of these three metrics, indicating that Superpoint, when augmented with CUDA, is the most effective solution. Moreover, among traditional algorithms, AKAZE demonstrates top-tier performance across the majority of evaluated metrics, making it a commendable choice.

C. Results of LiDAR-generated Image Keypoints Assisted LO

1) *Downsampled Point Cloud*: In Fig. ??, we demonstrate the sample result of the downsampled point cloud in Fig. ?? compared with the raw point cloud in Fig. ?. Notably, in the downsampled point cloud in Fig. ??, the red points are extracted based on signal images and the green ones are from range images. We draw the key points from both images to the signal image shown in the lower part of Fig. ??. The

disparity between the points extracted based on these two types of images shows the significance of different LiDAR-generated images. Additionally, in the preliminary evaluation of LO, we found the accuracy of LO is lower if we only integrated the signal images instead of both modalities. This encourages us to utilize both signal and range images in the latter part.

2) *LO based Evaluation*: In our experiment, various numbers of neighbor points are utilized, ranging from 3 to 7 for each type of LiDAR-generated image. We selected part of them to show the result here based on the principle that more accurate but less amount points. As we found in the previous section, the Superpoint has reliable key points detected, so we utilize this DL method to extract key points in our proposed approach while KISS-ICP is the point cloud registration and LO method. Table VI shows the performance of LO based on different sizes of neighbor point sizes in both indoor (Lab space, Hall) and outdoor (Open road and Forest) environments.

TABLE VI: Performance evaluation of LO (KISS-ICP) with raw point cloud and our downsampled point cloud, ‘Sig’ and ‘Rng’ represent the size of neighboring point areas for the signal and range images, respectively, denoted as *Sig_Rng*.

Neighbor Size (<i>Sig_Rng</i>)	Open road	Forest	Lab space (hard)	Lab space (easy)	Hall (large)
			(Translation error (mean/rmse)(m), rotation error(deg))		
4_4	N / A	(0.0790/0.090, 6.58)	(0.0520/0.062, 1.44)	(0.0270/0.031, 0.99)	(1.111/1.274, 3.37)
4_5	N / A	(0.0860/0.096, 7.22)	(0.0430/0.051, 1.51)	(0.0310/0.035, 1.05)	(0.724/0.819, 2.95)
4_7	(0.817/0.952, 2.33)	(0.0820/0.102, 7.78)	(0.0390/0.046, 1.46)	(0.0280/0.033, 0.98)	(0.583/0.660, 2.88)
5_4	(1.724/2.038, 2.10)	(0.0850/0.100, 6.81)	(0.0590/0.070, 1.71)	(0.0250/0.028, 0.98)	(1.065/1.242, 2.73)
5_5	(2.176/2.410, 1.76)	(0.1080/0.203, 6.96)	(0.0370/0.043, 1.35)	(0.0280/0.032, 0.97)	(0.707/0.801, 2.66)
5_7	(1.298/1.443, 2.71)	(0.0760/0.084, 6.11)	(0.0640/0.075, 1.54)	(0.0250/0.028, 0.94)	(0.676/0.746, 3.67)
7_4	(1.696/1.888, 2.31)	(0.0820/0.094, 6.98)	(0.0740/0.085, 1.64)	(0.0270/0.032, 0.99)	(0.806/0.917, 3.88)
7_5	(1.784/2.006, 2.30)	(0.0800/0.102, 7.72)	(0.0330/0.047, 1.59)	(0.0250/0.028, 0.97)	(0.698/0.803, 3.11)
Raw PC	N / A	(0.057/0.073, 8.91)	N / A	(0.020/0.022, 0.62)	N / A

As shown in Table VI, in the scenarios of Open road, Lab space (hard), and Hall(Large), the LO from KISS-ICP applying raw point cloud can not work properly with large drift which the error can not be calculated. Meanwhile, our proposed approach works all the time. Additionally, even when applying raw point cloud to KISS-ICP works, our approach can achieve comparable translation state estimation while more robust in the rotation state estimation across most of the situations.

In outdoor settings, a neighbor size 4_7 (4×4 for signal images and 7×7 for range images) exhibits notable efficacy in both translation and rotation state estimation. Conversely, in indoor environments, a neighbor size 5_5 (5×5 for signal images and 5×5 for range images) demonstrates commendable performance in the estimation of translation and rotation states, in addition to exhibiting efficient downsampling capabilities, as delineated in Table VI.

Based on the above result, we apply the neighbor size 4_7 for outdoor settings and the neighbor size 5_5 for indoor settings to further extend the performance evaluation by including the conventional keypoint detector approach and another point cloud matching approach, NDT. It is worth noting that the purpose of applying NDT here is not to compare with KISS-ICP but to show the generalization of our proposed approach among other point cloud registration methods.

The result in Table. VIII and Table. IX proves that the conventional keypoint extractor can achieve comparable LO

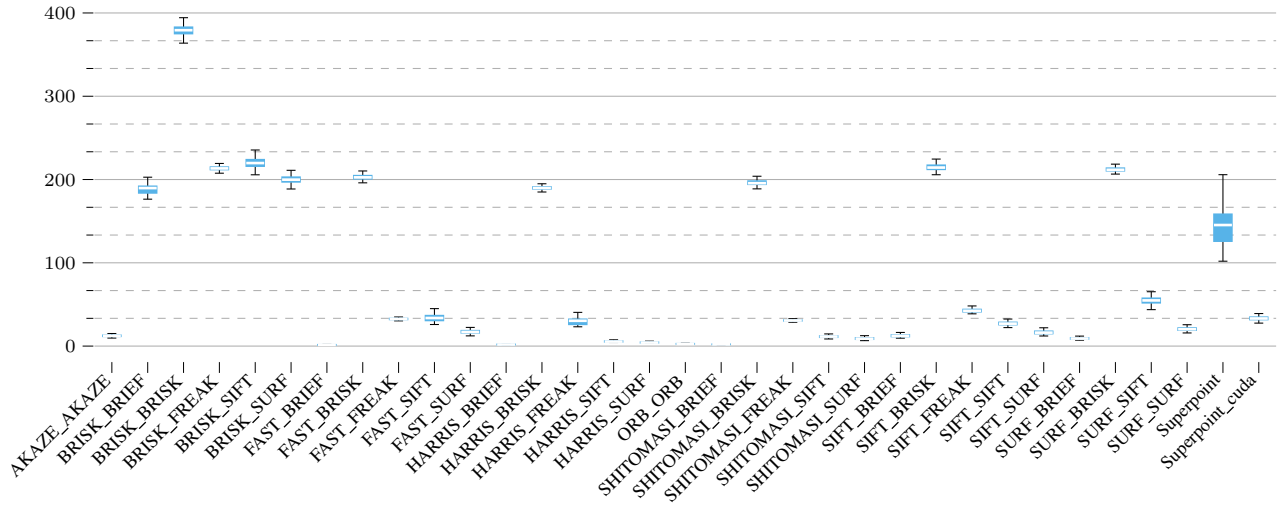
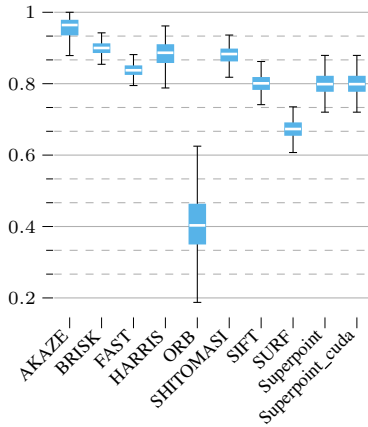
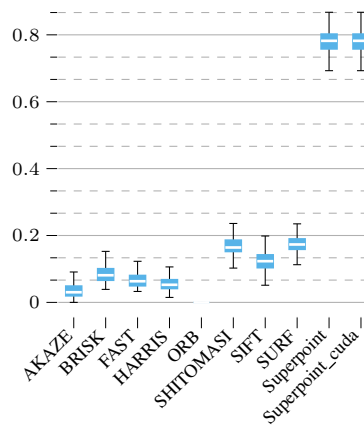


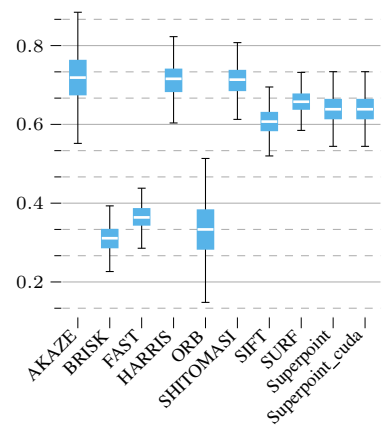
Fig. 6: Computational efficiency



(a) Rotation



(b) Scaling



(c) Noise Interference

Fig. 7: Robustness of the detector.

TABLE VII: The number of points left after downsampling with varied neighbor size, ‘Sig’ and ‘Rng’ represent the size of neighboring point areas for the signal and range images, respectively, denoted as *Sig_Rng*.

Neighbor Size (<i>Sig_Rng</i>)	Open road	Forest	Lab space (hard) Number of points(pts)	Lab space (easy)	Hall (large)
4_4	2650	7787	6435	6360	4742
4_5	3206	7812	6416	6302	4792
4_7	4784	11447	9518	9392	7094
5_4	3182	7843	6409	6333	4776
5_5	3183	7568	6446	6292	4783
5_7	4763	11519	9513	9386	7066
7_4	4760	11631	9445	9356	7070
7_5	4756	11627	9469	9378	7078
Raw PC	131072	131072	131072	131072	131072

translation estimation and more accurate rotation estimation to Superpoint. This performance is obtained with much less CPU and memory utilization, and fewer cloud points, but higher odometry publishing rates. Similar results are achieved by NDT based approach which validates the above result in a certain way. Notably, the memory consumption using KISS-

ICP with raw point cloud in Table. VIII is lower than others. As our observation indicates, the primary reason behind this is the drift, resulting in few points for the point cloud registration.

TABLE VIII: Evaluation of LO based on conventional and DL keypoint detectors with KISS-ICP

Evaluation Indicators	Approaches					
	Outdoor			Indoor		
	AKAZE	Superpoint	Raw PC	AKAZE	Superpoint	Raw PC
Translation Error (<i>m</i>)	0.096/0.107	0.082/0.102	N / A	0.092/0.099	0.037/0.043	N / A
Rotation error (<i>deg</i>)	4.27	7.78	N / A	1.22	1.71	N / A
CPU (%)	263.16	457.59	544.61	82.57	425.93	572.50
Mem (<i>MB</i>)	247.62	308.67	165.73	198.27	232.85	84.37
Avg Pts	4849	11447	131072	1176	6446	131072
Odom Rate (<i>Hz</i>)	10.0	4.0	2.95	10.0	7.6	2.82

TABLE IX: Evaluation of LO based on conventional and DL keypoint detectors with NDT

Evaluation Indicators	Approaches					
	Outdoor			Indoor		
	AKAZE	Superpoint	Raw PC	AKAZE	Superpoint	Raw PC
Translation Error (<i>m</i>)	0.115/0.126	0.090/0.098	N / A	0.102/0.114	0.054/0.071	N / A
Rotation error (<i>deg</i>)	4.84	5.66	N / A	1.15	1.31	N / A
CPU (%)	100.39	325.69	571.12	82.20	338.54	581.30
Mem (<i>MB</i>)	285.06	548.16	705.43	253.95	290.34	645.21
Avg Pts	4849	11447	131072	1176	6446	131072
Odom Rate (<i>Hz</i>)	10.0	4.6	3.34	10	8.21	1.20

V. CONCLUSION AND FUTURE WORK

To mitigate computational overhead while ensuring the retention of a sufficient number of dependable key points for point cloud registration in LO, this study introduces a novel approach that incorporates LiDAR-generated images. A comprehensive analysis of keypoint detection and descriptors, originally designed for conventional images, is conducted on the LiDAR-generated image. This not only informs subsequent sections of this paper but also sets the stage for future research endeavors aimed at enhancing the robustness and resilience of LO and SLAM technology. Building upon the insights gleaned from this analysis, we propose a methodology for down-sampling the raw point cloud while preserving the integrity of salient points. Our experiments demonstrate that our proposed approach exhibits comparable performance to utilizing the complete raw point cloud and, notably, surpasses it in scenarios where the full raw point cloud proves ineffective, such as in cases of drift. Additionally, our approach exhibits commendable robustness in the face of rotational transformations. The computation overhead of our approach is lower than the LO utilizing raw point cloud but with a higher odometry publishing rate.

In future work, there is potential to seamlessly integrate the current LiDAR-generated image keypoint extraction process into the broader SLAM pipeline. For instance, one avenue of exploration could involve amalgamating features extracted from LiDAR-generated images with those derived from point cloud data, facilitating the development of a lightweight SLAM system complemented by additional sensors, such as an IMU.

ACKNOWLEDGMENT

This research was supported by the Research Council of Finland's AeroPolis project (Grant 442 No. 348480) and RoboMesh project (Grant No. 336061).

REFERENCES

- [1] Li Qingqing, Yu Xianjia, Jorge Peña Queralta, and Tomi Westerlund. Multi-modal lidar dataset for benchmarking general-purpose localization and mapping algorithms. In *2022 IEEE/RSJ International Conference on Intelligent Robots and Systems (IROS)*, pages 3837–3844, 2022.
- [2] Ha Sier, Qingqing Li, Xianjia Yu, Jorge Peña Queralta, Zhuo Zou, and Tomi Westerlund. A benchmark for multi-modal lidar slam with ground truth in gnss-denied environments. *Remote Sensing*, 15(13):3314, 2023.
- [3] Chris Harris, Mike Stephens, et al. A combined corner and edge detector. In *Alvey vision conference*, volume 15, pages 10–5244. Citeseer, 1988.
- [4] Hans Moravec. Obstacle avoidance and navigation in the real world by a seeing robot rover. Technical report, Carnegie Mellon University, Pittsburgh, PA, September 1980.
- [5] Nilanjan Dey, Pradipti Nandi, Nilanjana Barman, Debolina Das, and Subhabrata Chakraborty. A comparative study between moravec and harris corner detection of noisy images using adaptive wavelet thresholding technique. *arXiv preprint arXiv:1209.1558*, 2012.
- [6] Jianbo Shi and Tomasi. Good features to track. In *1994 Proceedings of IEEE Conference on Computer Vision and Pattern Recognition*, pages 593–600, 1994.
- [7] Edward Rosten and Tom Drummond. Machine learning for high-speed corner detection. In *Computer Vision–ECCV 2006: 9th European Conference on Computer Vision, Graz, Austria, May 7–13, 2006. Proceedings, Part I* 9, pages 430–443. Springer, 2006.
- [8] Michael Calonder, Vincent Lepetit, Christoph Strecha, and Pascal Fua. Brief: Binary robust independent elementary features. In Kostas Daniilidis, Petros Maragos, and Nikos Paragios, editors, *Computer Vision – ECCV 2010*, pages 778–792, Berlin, Heidelberg, 2010. Springer Berlin Heidelberg.
- [9] Alexandre Alahi, Raphael Ortiz, and Pierre Vanderghyest. Freak: Fast retina keypoint. In *2012 IEEE Conference on Computer Vision and Pattern Recognition*, pages 510–517, 2012.
- [10] David G. Lowe. Distinctive image features from scale-invariant keypoints. *International Journal of Computer Vision*, 60:91–110, 2004.
- [11] D.G. Lowe. Object recognition from local scale-invariant features. In *Proceedings of the Seventh IEEE International Conference on Computer Vision*, volume 2, pages 1150–1157 vol.2, 1999.
- [12] Herbert Bay, Tinne Tuytelaars, and Luc Van Gool. Surf: Speeded up robust features. In Aleš Leonardis, Horst Bischof, and Axel Pinz, editors, *Computer Vision – ECCV 2006*, pages 404–417, Berlin, Heidelberg, 2006. Springer Berlin Heidelberg.
- [13] Stefan Leutenegger, Margarita Chli, and Roland Y. Siegwart. Brisk: Binary robust invariant scalable keypoints. In *2011 International Conference on Computer Vision*, pages 2548–2555, 2011.
- [14] Ethan Rublee, Vincent Rabaud, Kurt Konolige, and Gary Bradski. Orb: An efficient alternative to sift or surf. In *2011 International conference on computer vision*, pages 2564–2571. Ieee, 2011.
- [15] Pablo Fernández Alcantarilla, Jesús Nuevo, and Adrien Bartoli. Fast explicit diffusion for accelerated features in nonlinear scale spaces. In *British Machine Vision Conference*, 2013.
- [16] Xin Yang and K.-T. Tim Cheng. Local difference binary for ultrafast and distinctive feature description. *IEEE transactions on pattern analysis and machine intelligence*, 36:188–194, 01 2014.
- [17] Mahmoud Hassaballah and Ali Ismail Awad. *Deep learning in computer vision: principles and applications*. CRC Press, 2020.
- [18] Ross Girshick. Fast r-cnn. In *Proceedings of the IEEE international conference on computer vision*, pages 1440–1448, 2015.
- [19] Daniel DeTone, Tomasz Malisiewicz, and Andrew Rabinovich. Superpoint: Self-supervised interest point detection and description. In *Proceedings of the IEEE conference on computer vision and pattern recognition workshops*, pages 224–236, 2018.
- [20] Tao Wu, Hao Fu, Bokai Liu, Hanzhang Xue, Ruike Ren, and Zhiming Tu. Detailed analysis on generating the range image for lidar point cloud processing. *Electronics*, 10(11):1224, 2021.
- [21] Point Cloud Library. How to create a range image from a point cloud. Accessed on September 13, 2023.
- [22] Ardi Tampuu, Romet Aidla, Jan Aare van Gent, and Tabet Matiisen. Lidar-as-camera for end-to-end driving. *Sensors*, 23(5), 2023.
- [23] Angus Pacala. Lidar as a camera – digital lidar’s implications for computer vision. *Ouster Blog*, 2018.
- [24] Maria Tsiourva and Christos Papachristos. Lidar imaging-based attentive perception. In *2020 International Conference on Unmanned Aircraft Systems (ICUAS)*, pages 622–626, 2020.
- [25] Ha Sier, Xianjia Yu, Iacopo Catalano, Jorge Peña Queralta, Zhuo Zou, and Tomi Westerlund. Uav tracking with lidar as a camera sensor in gnss-denied environments. In *2023 International Conference on Localization and GNSS (ICL-GNSS)*, pages 1–7. IEEE, 2023.
- [26] Xianjia Yu, Sahar Salimpour, Jorge Peña Queralta, and Tomi Westerlund. General-purpose deep learning detection and segmentation models for images from a lidar-based camera sensor. *Sensors*, 23(6):2936, 2023.
- [27] Xieyuanli Chen, Ignacio Vizzo, Thomas Labe, Jens Behley, and Cyrill Stachniss. Range image-based lidar localization for autonomous vehicles. In *2021 IEEE International Conference on Robotics and Automation (ICRA)*, pages 5802–5808, 2021.
- [28] Jared Heinly, Enrique Dunn, and Jan-Michael Frahm. Comparative evaluation of binary features. In *European Conference on Computer Vision*, 2012.
- [29] Krystian Mikolajczyk, Tinne Tuytelaars, Cordelia Schmid, Andrew Zisserman, Jiri Matas, Frederik Schaffalitzky, Timor Kadir, and Luc Van Gool. A comparison of affine region detectors. *International Journal of Computer Vision*, 65:43–72, 11 2005.
- [30] Shaharyar Ahmed Khan Tareen and Zahra Saleem. A comparative analysis of sift, surf, kaze, akaze, orb, and brisk. In *2018 International Conference on Computing, Mathematics and Engineering Technologies (iCoMET)*, pages 1–10, 2018.
- [31] Andreas Geiger, Philip Lenz, Christoph Stiller, and Raquel Urtasun. Vision meets robotics: The kitti dataset. *International Journal of Robotics Research (IJRR)*, 2013.

- [32] Vassileios Balntas, Karel Lenc, Andrea Vedaldi, and Krystian Mikolajczyk. Hpatches: A benchmark and evaluation of handcrafted and learned local descriptors. In *CVPR*, 2017.
- [33] Dibyendu Mukherjee, Q. M. Jonathan Wu, and Guanghui Wang. A comparative experimental study of image feature detectors and descriptors. *Machine Vision and Applications*, 26:443–466, 05 2015.
- [34] C. Strecha, W. von Hansen, L. Van Gool, P. Fua, and U. Thoennessen. On benchmarking camera calibration and multi-view stereo for high resolution imagery. In *2008 IEEE Conference on Computer Vision and Pattern Recognition*, pages 1–8, 2008.
- [35] David Bojanić, Kristijan Bartol, Tomislav Pribanic, Tomislav Petković, Yago Diez, and Joaquim Mas. On the comparison of classic and deep keypoint detector and descriptor methods. pages 64–69, 09 2019.
- [36] Christoph Sager, Christian Janiesch, and Patrick Zschech. A survey of image labelling for computer vision applications. *Journal of Business Analytics*, 4(2):91–110, 2021.
- [37] Christopher J. Rapson, Boon-Chong Seet, M. Asif Naeem, Jeong Eun Lee, Mahmoud Al-Sarayreh, and Reinhard Klette. Reducing the pain: A novel tool for efficient ground-truth labelling in images. In *2018 International Conference on Image and Vision Computing New Zealand (IVCNZ)*, pages 1–9, 2018.
- [38] Xu Wang, Yi Jin, Yigang Cen, Tao Wang, Bowen Tang, and Yidong Li. Lightn: Light-weight transformer network for performance-overhead tradeoff in point cloud downsampling. *arXiv preprint arXiv:2202.06263*, 2022.
- [39] Bochang Zou, Huadong Qiu, and Yufeng Lu. Point cloud reduction and denoising based on optimized downsampling and bilateral filtering. *Ieee Access*, 8:136316–136326, 2020.
- [40] Ji Zhang and Sanjiv Singh. Loam: Lidar odometry and mapping in real-time. In *Robotics: Science and systems*, volume 2, pages 1–9. Berkeley, CA, 2014.
- [41] Tixiao Shan and Brendan Englot. Lego-loam: Lightweight and ground-optimized lidar odometry and mapping on variable terrain. In *2018 IEEE/RSJ International Conference on Intelligent Robots and Systems (IROS)*, pages 4758–4765. IEEE, 2018.
- [42] Han Wang, Chen Wang, Chun-Lin Chen, and Lihua Xie. F-loam: Fast lidar odometry and mapping. In *2021 IEEE/RSJ International Conference on Intelligent Robots and Systems (IROS)*, pages 4390–4396. IEEE, 2021.
- [43] Paul J Besl and Neil D McKay. Method for registration of 3-d shapes. In *Sensor fusion IV: control paradigms and data structures*, volume 1611, pages 586–606. Spie, 1992.
- [44] Kenji Koide, Masashi Yokozuka, Shuji Oishi, and Atsuhiko Banno. Voxelized gicp for fast and accurate 3d point cloud registration. In *2021 IEEE International Conference on Robotics and Automation (ICRA)*, pages 11054–11059. IEEE, 2021.
- [45] Pierre Dellenbach, Jean-Emmanuel Deschaud, Bastien Jacquet, and François Goulette. Ct-icp: Real-time elastic lidar odometry with loop closure. In *2022 International Conference on Robotics and Automation (ICRA)*, pages 5580–5586. IEEE, 2022.
- [46] Ignacio Vizzo, Tiziano Guadagnino, Benedikt Mersch, Louis Wiesmann, Jens Behley, and Cyrill Stachniss. Kiss-icp: In defense of point-to-point icp—simple, accurate, and robust registration if done the right way. *IEEE Robotics and Automation Letters*, 8(2):1029–1036, 2023.
- [47] Peter Biber and Wolfgang Straßer. The normal distributions transform: A new approach to laser scan matching. In *Proceedings 2003 IEEE/RSJ International Conference on Intelligent Robots and Systems (IROS 2003)(Cat. No. 03CH37453)*, volume 3, pages 2743–2748. IEEE, 2003.